Chemistry Journals

Analytical, Inorganic, Organic, Physical, Materials Science

Analysis of protein-heparin interactions using a portable SPR instrument

Dunhao Su [Equal first author, 1] , **Yong Li** [Equal first author, 1] , **Edwin A Yates** [1] , **Mark A Skidmore** [2] , **Marcelo A Lima** [2] , **David G Fernig** Corresp. [1]

[1] Biochemistry, University of Liverpool, Liverpool, United Kingdom

[2] Molecular & Structural Biosciences, School of Life Sciences, University of Keele, Newcastle-Under-Lyme, United Kingdom

Corresponding Author: David G Fernig
Email address: dgfernig@liv.ac.uk

Optical biosensors such as those based on surface plasmon resonance (SPR) are a key analytical tool for understanding biomolecular interactions and function as well as the quantitative analysis of analytes in a wide variety of settings. The advent of portable SPR instruments enables analyses in the field. A critical step in method development is the passivation and functionalisation of the sensor surface. We describe the assembly of a surface of thiolated oleyl ethylene glycol/biotin oleyl ethylene glycol and its functionalisation with streptavidin and reducing end biotinylated heparin for a portable SPR instrument. Such surfaces can be batch prepared and stored. Two examples of the analysis of heparin-binding proteins are presented. The binding of fibroblast growth factor2 and competition for the binding of a heparan sulfate sulfotransferase by a library of selectively modified heparins and suramin, which identify the selectivity of the enzyme for sulfated structures in the polysaccharide and demonstrate suramin as a competitor for the enzyme's sugar acceptor site. Heparin functionalised surfaces should have a wide applicability, since this polysaccharide is a close structural analogue of the host cell surface polysaccharide, heparan sulfate, a receptor for many endogenous proteins and viruses.

1 **Analysis of protein-heparin interactions using a**
2 **portable SPR instrument**
3

5 Dunhao Su*[1], Yong Li*[1], Edwin A. Yates[1], Mark A. Skidmore[2], Marcelo A. Lima[2] and David G.
6 Fernig[1]
7 [1] Department of Biochemistry and Systems Biology, Institute of Integrative, Molecular and
8 Systems Biology, Biosciences Building, University of Liverpool, Liverpool L69 7ZB, United
9 Kingdom.
10 [2] Molecular & Structural Biosciences, School of Life Sciences, Keele University, Newcastle-
11 Under-Lyme, Staffordshire, ST5 5BG, United Kingdom.
12
13 *Equal first author
14 Corresponding Author:
15 David G. Fernig[1]
16 Department of Biochemistry and Systems Biology, Institute of Integrative, Molecular and
17 Systems Biology, Biosciences Building, University of Liverpool, Liverpool L69 7ZB, United
18 Kingdom
19 Email address: dgfernig@liv.ac.uk

21 ## Abstract

22 **Optical biosensors such as those based on surface plasmon resonance (SPR) are a key**
23 **analytical tool for understanding biomolecular interactions and function, as well as the**
24 **quantitative analysis of analytes in a wide variety of settings. The advent of portable SPR**
25 **instruments enables analyses in the field. A critical step in method development is the**
26 **passivation and functionalisation of the sensor surface. We describe the assembly of a**
27 **surface of thiolated oleyl ethylene glycol/biotin oleyl ethylene glycol and its**
28 **functionalisation with streptavidin and reducing end biotinylated heparin for a portable**
29 **SPR instrument. Such surfaces can be batch prepared and stored. Two examples of the**
30 **analysis of heparin-binding proteins are presented. The binding of fibroblast growth**
31 **factor2 and competition for the binding of a heparan sulfate sulfotransferase by a library**
32 **of selectively modified heparins and suramin, which identify the selectivity of the enzyme**
33 **for sulfated structures in the polysaccharide and demonstrate suramin as a competitor**
34 **for the enzyme's sugar acceptor site. Heparin functionalised surfaces should have a wide**
35 **applicability, since this polysaccharide is a close structural analogue of the host cell**
36 **surface polysaccharide, heparan sulfate, a receptor for many endogenous proteins and**
37 **viruses.**
38

39 ## Introduction

40   The regulation of biochemical processes depends on the dynamic interactions of biological

41   molecules. The characterisation of these interactions represents an important step in gaining an

42   understanding of function and how this may be perturbed in a biological experiment. Moreover,

43   the ability of biological molecules such as antibodies and receptors, as well as various host

44   entities, to recognise molecular partners with high selectivity has become integral to

45   (bio)analytical techniques. A large number of different surface measurement platforms have been

46   adapted for such analyses and of these, surface plasmon resonance and related techniques are

47   some of the most popular, perhaps due to their early commercialisation (Brigham-Burke et al.

48   1992; Watts et al. 1994), rapidity and the ease of measurement. The technique has since evolved

49   to encompass both analysis of functional molecular interactions and quantification of the amount

50   of an analyte in a sample. The recent development of portable, low-cost instrumentation, e.g.,

51   (Zhao et al. 2015), has substantially increased the reach of the technique. In an SPR

52   measurement, the ligand is immobilised on the sensor surface and the analyte is usually flowed

53   over the sensor, though some systems do not use fluidics. The instruments use changes in the

54   refractive index near the surface to measure in real-time the interactions of analyte with ligand.

55   Like any analytical method, SPR has limitations. One relates to the surface itself, while fluidics

56   systems, which are characterised by inefficient exchange between the bulk, flowing liquid and

57   the stationary layer, are a source of further artefacts. These have been reviewed extensively e.g.,

58   (Schuck & Zhao 2010). Another limitation relates to signal and noise. The principal source of

59   noise is the interaction of the analyte with the surface to which the ligand is immobilised. Thus,

60   an important part of experimental design is the synthesis of surfaces suitable for capturing

61   ligands that exhibit very low analyte binding. Gold binds many groups that include thiols, amines

62   and carbonyls, so has to be passivated. Dextran-based hydrogels were an early solution, but these

63   are prone to high non-specific binding, as well as to generating artefacts arising from the collapse

64   or expansion of the hydrogel upon interaction with an analyte (Schuck & Zhao 2010). Since

65   then, substantial advances involving useful cross-fertilisation between nanoparticle and surface

66   sensing fields have been made in passivating gold surfaces with self-assembled monolayers

67   (SAMs). These approaches include mercaptoproprionic acid (Mauriz et al. 2006), supported lipid

68   bilayers (Ferhan et al. 2019; Marques et al. 2014), peptides (Bolduc et al. 2009; Bolduc et al.

69   2011; Bolduc et al. 2010) and thiolated oleyl ethylene glycol (OEG) (Migliorini et al. 2014).

70   SAMs have many advantages; in particular, functionalisation can be achieved in the same step as

71   passivation by the inclusion of a mole percent of a functional ligand. This allows statistical

72   control of the functionalisation of the SAM and thereby the surface. Control of the surface

73   density of functionalisation provides a means by which steric hindrance artefacts can be avoided

74   (Edwards et al. 1995). Since the SAMs consist of small molecules, the immobilised ligand will

75   also be close to the surface. Thus, a SAM affords greater sensitivity than a hydrogel, because the

76   SPR signal decreases exponentially with the distance from the surface. No passivation system

77   offers a universal panacea, however, so having access to several distinct SAMs increases the

78   probability of finding a surface suitable for a particular measurement.

79   We have adapted an existing strategy for the functionalisation of gold surfaces with a monolayer

80   of streptavidin that is particularly resistant to non-specific binding (Migliorini et al. 2014) to the

81   SPR chips of a portable SPR instrument (Zhao et al. 2015). Self-assembled monolayers of

82   defined mixtures of thiolated oleyl ethylene glycol (OEG) and biotin OEG were synthesised on

83   the gold surface and used to capture streptavidin. Reducing-end biotinylated heparin (Thakar et

84   al. 2014) was then captured on the streptavidin surface. Heparin is a convenient experimental

85   proxy for the sulfated domains of cellular heparan sulfate, which by virtue of the latter's more

86   than 800 extracellular protein partners is a major regulator of cell function in development,

87   homeostasis and disease (Nunes et al. 2019). Indeed, this surface has recently been used to

88   characterise the interaction of the spike protein of SARS-CoV-2 with heparin (Mycroft-West et

89   al. 2020). Here we provide an in-depth description of the preparation of this surface, benchmark

90   it against the well-characterised interaction of fibroblast growth factor-2 (FGF2) with heparin

91   (Rahmoune et al. 1998) and demonstrate its application in the characterisation of heparan sulfate

92   sulfotransferases, in this instance a fusion protein of glutathione-S-transferase (GST) and 3-O

93   heparan sulfate sulfotransferase 3A1 (HS3ST3A1). We demonstrate that suramin, a previously

94   characterised inhibitor of HS2ST1 that was postulated to compete for both the donor and

95   acceptor sites of the enzyme (Byrne et al. 2018b), did indeed compete with GST-HS3ST3A1

96   binding to heparin. Additionally, the OEG/biotin OEG surfaces can be stored and re-used, and

97   complement the existing peptide surfaces (Bolduc et al. 2009; Bolduc et al. 2011; Bolduc et al.

98   2010) that have been published for this portable SPR instrument.

99

100 **Materials & Methods**

101 **Materials**

102   The chemically modified heparins (Table 1) were produced and characterised as described

103   (Yates et al. 1996). Human fibroblast growth factor 2 (FGF2) and was produced as described by

104   Duchesne et al.(Duchesne et al. 2012).

105   Oxime biotinylation of heparin at the reducing end

106   Porcine intestinal heparin (H4784, Sigma) was biotinylated at the reducing end using

107   hydroxylamine biotin, as described by Thakar et al.,(Thakar et al. 2014), as this provides for a

108   stable product. Heparin (4 mM) was reacted with 4 mM N-(aminooxyacetyl)-N'-(D-Biotinoyl)

109   hydrazine, (A10550, ThermoFisher Scientific, UK) in 100 mM aniline and 100 mM acetate

110   buffer, pH4.6, total volume 120 µl, at 37 °C for 48 hours. After, unreacted biotin was removed

111   and the buffer exchanged to PBS (Thermo Scientific Oxoid, phosphate-buffered saline tablets,

112   BR0014G) by six rounds of filtration at 10,000 g for 10 min in a 3k MWCO centrifugal filter

113   (ThermoFisher Scientific, 88512). The concentration of biotin-heparin was then measured using

114   the carbazole assay. Briefly, 50 µL of 10-fold dilution of the biotin-heparin and a range of

115   heparin standards at known concentration were added to a 96-well-plate, followed by the

116   addition of 200 µL H_2SO_4 and then incubated at 98 °C for 20 min. After cooling to room

117   temperature over 10 min, 20 µL of 1.25 mg/mL carbazole was added to the wells, which were

118   then incubated at 98 °C for 10 min. After cooling to room temperature for 10 min the absorbance

119   in the wells was measured at 535 nm, with the heparin standard curve enabling quantification of

120   the biotin-heparin.

121   Expression and Purification of GST-HS3ST3A1

122   A cDNA fragment encoding the catalytic domain of human HS3ST3A1 (Uniprot accession

123   Q9Y663, residues 139-406, purchased from Thermo Fisher, UK) was cloned into the pGEX4T3

124   vector using EcoRI and NotI. Glutathione-S-transferase- (GST) HS3ST3A1 was expressed and

125   purified following published procedures for GST-HS3ST3A1 (Moon et al. 2004) and GST-

126   HS3ST1 (Wheeler et al., 2021) fusion proteins. Protein was expressed in C41 (DE3) *E. coli*,

127   induced with 200 µM isopropyl 1-thio-ß-D-galactopyranoside (IPTG) at 22°C overnight.

128   Following centrifugation (15 min, 4,150x g) and resuspension in lysis buffer (100 mM NaCl, 50

129   mM Tris-Cl, pH 7.4) cells were lysed by sonication (six 1 min 30 s cycles of sonication on ice)

130   and the lysate cleared by centrifugation (45 min, 38 000 g). Soluble GST-HS3ST3A1 in the

131   supernatant was purified by application to a 2 mL glutathione resin (Genscript Biotech

132   Corporation, Netherlands), washing with 100 mM NaCl, 50 mM Tris, pH 7.4 and eluting with 10

133 mM reduced glutathione, 100 mM NaCl, 50 mM Tris, pH 7.4. The eluate was immediately

134 applied to a 1 mL heparin (Affi-Gel hep, Bio-Rad, UK) column, washed with 50 mM NaCl, 50

135 mM Tris, pH 7.4, and eluted with 600 mM NaCl, 50 mM Tris, pH 7.4 (Supplementary Fig. 1).

136 The specific extinction coefficient for GST-HS3ST3A1 at 280 nm, calculated from its amino

137 acid sequence was used for quantification and protein was snap frozen in liquid nitrogen and

138 stored in aliquots at -80°C.

139 **Preparation of functionalised gold surfaces**

140 The functionalisation of the gold sensor surface was based on an existing method (Migliorini et

141 al. 2014). The detailed protocol for this is available at protocols.io (Su & Fernig 2021). Briefly,

142 mixtures of thiolated oleyl ethylene glycol (OEG) and thiolated oleyl ethylene glycol-biotin

143 (OEG-biotin) at the stated % mole/mole and at a final concentration of 100 mM were prepared in

144 ethanol. A plasma cleaned gold SPR sensor chip was incubated in this solution for 36 h to form

145 an OEG/OEG-biotin SAM. The sensor chip was washed in ethanol and could be stored at 4 °C in

146 ethanol for at least 3 months. The sensor chip placed in the P4SPR, multi-channel SPR

147 instrument (Affinté Instruments; Montréal, Canada) and the three measurement channels and the

148 control, background channel, were then equilibrated in PBS at a flow rate of 500 µL/min using

149 an Ismatec peristaltic pump. A high flow rate was chosen to minimize mass transport limitations

150 (Schuck & Zhao 2010), which are particularly acute when molecular interactions are driven by

151 electrostatic interactions, as for proteins binding heparin, though lower flow rates are often

152 appropriate, depending on the characteristics of the interaction and the assay. All subsequent

153 steps used this flow rate. After equilibration in PBS, streptavidin (Sigma), 1 mg/mL in PBS was

154 injected over the four channels. Often a second injection of streptavidin was performed to

155 determine whether the surfaces were fully functionalised. Streptavidin not specially bound to

156 biotin was removed by two regeneration steps, the first using 2 M NaCl, the second 20 mM HCl.

157 Then 1 mL, 90 µg/mL biotinylated heparin was injected over the three measurement channels.

158 Again, a repeat injection of biotinylated heparin was performed to see if the streptavidin in the

159 three measurement channels was fully derivatised. Finally, the three measurement channels were

160 regenerated by sequential 1 mL injections of 2 M NaCl and 20 mM HCl (Fig. 1). The heparin

161 functionalised surfaces could be stored in PBS at 4 °C for at least 10 days.

162 **Measurement of protein-heparin interactions**

163   All measurements of the binding of protein analytes to immobilised heparin used PBS

164   supplemented with 0.01% (v/v) Tween 20 (PBST) as the running buffer, to prevent adsorption of

165   analyte to the fluidics, at a flow rate of 500 µL/min. FGF2 and HS3ST3A were injected over the

166   three measurement channels and the control channel at the concentrations indicated in the figure

167   legends. The biotin-heparin surfaces were regenerated with 1 mL injections of 2 M NaCl and 20

168   mM HCl or 0.25 % (w/v) SDS and 20 mM HCl. In some experiments the protein analyte was

169   pre-mixed with a potential competitor for its binding to heparin prior to injection.

170

Results and Discussion

172   SAMs of thiolated OEG:thiolated biotin OEG functionalised with streptavidin on gold have

173   been shown to be very resistant to non-specific binding and have been extensively characterised

174   in terms of areal density of immobilized streptavidin and biotinylated polysaccharides

175   (Migliorini et al. 2014). This approach also allows control of the surface density of streptavidin

176   and hence biotinylated ligand immobilised on the surface by simply controlling the molar

177   stoichiometry of thiolated OEG: thiolated biotin OEG (Fig. 1). Moreover, by capturing a

178   biotinylated ligand, its orientation can be pre-determined if the biotinylation reaction is selective.

179   Combined, these features reduce the likelihood of artefacts associated with diffusion in fluidics

180   systems (Schuck & Zhao 2010) and steric hindrance of the binding site(s) of the immobilised

181   ligand (Edwards et al. 1995). Three (mole/mole) ratios were chosen, 1 %, 0.3 % and 0.1 %.

182   Assuming equal probability of incorporation of the thiolated biotin OEG into the monolayer and

183   a diameter of streptavidin of ~5.5 nm, these should yield, respectively, a very tightly packed

184   monolayer, a monolayer, and partial surface coverage of streptavidin.

185   Following plasma cleaning and incubation of the gold surfaces with the thiolated OEG / thiolated

186   biotin OEG mixture for 36 h, the surfaces were washed with ethanol. The OEG/biotin-OEG

187   SAMS were found to be stable for at least three months at 4 °C, which enabled batch preparation

188   of surfaces. The thiolated OEG surface was placed in the instrument and equilibrated in running

189   buffer (PBS, 500 µL/min), and then 1 mL streptavidin (20 µg/mL in PBS) was injected at the

190   same flow rate providing a final response of ~ 2 nm (Fig. 2A). The surface was then subjected to

191   a wash with 2 M NaCl and then 20 mM HCl (1 mL each) to remove any non-specifically bound

192   streptavidin. A second injection of streptavidin only resulted in a very small increase in bound

193   protein (Fig. 2A, red arrows, 800 min to 1100 min), indicating that the biotinylated OEG on the

194 surface was near saturated with streptavidin after the first injection. Nevertheless, all subsequent

195 surfaces were prepared with two sequential injections of streptavidin, to ensure that this was

196 indeed the case. The surface was again washed sequentially with 2 M NaCl and 20 mM HCl.

197 Biotinylated heparin (1 mL, 90 µg/mL) was then injected over the three measurement channels,

198 A-C. Only a small response was observed, as the refractive index of this sulfated polysaccharide

199 is at the lower limit of detection (Fig. 2B red arrows 1850 min to 2000 min). After washing the

200 surface with 2 M NaCl and 20 mM HCl, biotin heparin was again injected over the three

201 measurement channels, A-C, but this did not cause any further increase in signal, demonstrating

202 that the first single injection was sufficient to occupy the available sites on the immobilised

203 streptavidin. Following washes with 2 M NaCl and 20 mM HCl, the surface was returned to

204 running buffer. The heparin functionalised surfaces could be removed from the instrument and

205 stored at 4 °C in PBS for up to 10 days without any detectable loss of analyte binding.

206 To determine whether the amount of streptavidin immobilised on the surface could indeed be

207 controlled by changing the percentage thiolated OEG in the SAM, SAMs with three different

208 percentage thiolated biotin OEG were functionalised with streptavidin. The data demonstrate a

209 dependence of the level of streptavidin captured on the SAM and the percentage thiolated biotin

210 OEG in the original ligand mixture used to assemble the SAM (Fig. 1C). This in turn enables the

211 density of biotinylated immobilised ligand to be controlled. In the previous work, maximal areal

212 density of streptavidin was obtained with 0.1 % mole/mole thiolated biotin OEG (Migliorini et

213 al. 2014), but in the present work this did not afford anything like full coverage of the surface.

214 That 1% (mole/mole) is likely to do so is supported by several lines of evidence. Supported lipid

215 bilayers on glass require 5% mole/mole biotinylated lipid for full coverage by streptavidin,

216 which is higher than that obtained on the gold surface, likely due to be due to the mobility of the

217 lipids increasing the streptavidin's packing density (Migliorini et al. 2014). OEG is considerably

218 smaller than a lipid and with streptavidin occupying ~23 nm^2, then at 1% mole/mole thiolated

219 biotin OEG will be sufficient to provide a streptavidin monolayer. This monolayer will have

220 gaps, simply due to inefficient packing that are the consequence of the thiolated OEG molecules

221 being immobilized on the gold surface.

222 The heparin functionalised surfaces were then tested for FGF2 binding, as the interaction of this

223 growth factor with heparin has been well characterised, including the measurement of binding

224 kinetics in optical biosensors, e.g., (Delehedde et al. 2002). First the running buffer was changed

225   to PBST. FGF2 (1 mL, 100 nM) was injected over the three measurement channels, previously

226   functionalised with biotin heparin immobilised on streptavidin (Fig. 3A) and the control channel

227   (functionalised solely with streptavidin, Fig. 3A dotted line). There was little response in the

228   control channel indicating that, as previously observed, FGF2 did not bind streptavidin

229   (Rahmoune et al. 1998) or the underlying OEG SAM (Migliorini et al. 2014). In contrast, in the

230   measurement channels there was a significant response (~1.2 nm). When the channels were

231   returned to running buffer, the response was stable. The lack of dissociation (or very slow

232   dissociation) is a hallmark of the rebinding of a dissociated ligand before it can diffuse into the

233   flowing bulk solution (Schuck & Zhao 2010). Rebinding is particularly acute with interactions

234   possessing a significant electrostatic component, as is the case with protein-sulfated

235   glycosaminoglycan binding, since these have fast association rate constants due to electrostatic

236   steering. Rebinding can be overcome by injection of non-biotinylated ligand, in this case heparin

237   (Sadir et al. 1998). As expected, this resulted in a dissociation curve (Fig. 4A). Washing the

238   surface with 1 mL 2 M NaCl and then 20 mM HCl completely regenerated the surface, as the

239   baseline returned to its original value (Fig. 3A). The second 20 mM HCl regeneration step was

240   included to ensure both full regeneration of the surface and that no analyte remained associated

241   with the fluidics.

242   Recently, we have described two new assays for the identification of inhibitors of heparan sulfate

243   sulfotransferases (HSSTs) (Byrne et al. 2018b), the enzymes responsible for the sulfation of

244   precursors of heparan sulfate and heparin. These assays can measure whether a compound

245   interacts with a sulfotransferase resulting in a change to its thermal stability or the activity of the

246   sulfotransferase towards a model oligosaccharide substrate. The latter assay can also determine

247   whether the compound is competitive with 3'-phosphoadenosine-5'-phosphosulfate (PAPS), the

248   universal sulfate donor. However, this assay cannot determine whether a compound is competing

249   with the sugar acceptor, since the sulfation of the sugar acceptor is measured. Consequently, it

250   was of interest to determine whether it would be possible to develop SPR assays to explore the

251   selectivity of a HSST for particular patterns of sulfation of the sugar acceptor, and whether

252   heparin-binding might be used to identify likely acceptor competitors. When 50 nM HS3STA1

253   was injected over the control, streptavidin functionalised surface, the small response observed

254   returned to baseline as soon as the injection ended, and the surface had been returned to running

255   buffer (Fig. 3B, dotted line). This response is characteristic of a bulk shift, presumably arising

256   from the refractive index of the GST-HS3ST3A1 and its buffer being higher than that of running

257   buffer. Thus, HS3STA3A1 does not interact with streptavidin or the underlying OEG SAM.

258   Injection of GST-HS3ST3A1 over the heparin-derivatised surface resulted in a response of 0.5

259   nm (Fig. 3B). As observed with FGF2 (Fig. 3A), when the surface returned to running buffer,

260   there was little dissociation (Fig 3B). Again, dissociation could be induced by the injection of

261   heparin over the surface (Fig. 4B). The heparin-derivatised surface was successfully regenerated

262   with a wash with 2 M NaCl followed by one with 20 mM HCl (Fig. 3B). However, upon

263   multiple injections, a small, but measurable rise in baseline was sometimes observed, indicative

264   of incomplete removal of the bound analyte. Consequently, the surface was thereafter

265   regenerated with a wash of 0.25 % (w/v) SDS; a second wash with 20 mM HCl was undertaken

266   to ensure that no residual SDS was present on the fluidics or the surface (Fig. 3C). These latter

267   data demonstrate that 0.25 % (w/v) SDS does not remove bound SA or damage the OEG SAM,

268   but did afford full regeneration when many injections of the enzyme were performed.

269   We next examined the competition for GST-HS3ST3A1 binding to the heparin-derivatised

270   surface by soluble heparin. GST-HS3ST3A1 (50 nM final concentration) was pre-mixed with

271   heparin to yield the indicated final concentration. Samples were injected over the heparin-

272   derivatised surface and then regenerated with 2 M NaCl and 20 mM HCl prior to the next

273   injection. The data demonstrate dose-dependent inhibition of binding by soluble heparin with an

274   IC_{50} of under 0.34 µg/ml heparin (Fig. 5A). To identify sulfation patterns preferentially

275   recognised by GST-HS3ST3A1, competition assays using a library of modified heparins were

276   performed. Selective removal of sulfate groups to produce the different modified heparins (Table

277   1) was expected to reduce their inhibition of the binding of the enzyme to the immobilised

278   heparin, as seen previously with other heparin/HS binding proteins (Li et al. 2016).

279   Consequently, a final concentration for the heparin derivatives of 1.7 µg/mL was chosen, since

280   with the parent heparin, this provided close to 100% inhibition (Fig. 5A). Selective removal of

281   any one of the sulfate groups on heparin reduced somewhat the effectiveness of the derivative as

282   a competitor, although these different derivatives, D2 to D4, were not equivalent, indicating that

283   effective interaction also involved a degree of conformational compatibility. Thus, heparin

284   derivatives with sulfate at the C2 position of iduronate residue and sulfate at either the C6 or the

285   C2 positions of the glucosamine residue, D2 and D4, respectively, were nearly as successful

286   competitors as the parent heparin (Fig. 5B). In contrast, the heparin with sulfate at C2 and C6 of

287 glucosamine residues, D3, was a less effective inhibitor. These data indicate that GST-

288 HS3ST3A1 has a preference for a polysaccharide containing 2-*O* sulfated iduronate and either 6-

289 *O* or *N*-sulfated glucosamine. Loss of any two, or all three, sulfate groups resulted in heparin

290 derivatives that were less effective competitors (Fig. 5A). Persulfated heparin (D9) was as

291 effective a competitor as the parent heparin, but not more effective, which indicated that simple

292 charge density was not entirely responsible for the interaction. These data are consistent with the

293 observation that GST-HS3ST3A1 is a 'gD' HS 3-*O* sulfotransferase (Moon et al. 2004), which

294 sulfates the hydroxyl group at the C3 position of *N*-sulfated glucosamine residues in the context

295 of flanking 2-*O* sulfated iduronate residues, to produce structures that bind the gD protein of

296 herpes simplex virus (Moon et al. 2004).

297 Suramin, one of the compounds identified in a recent screen of inhibitors of HS2ST1 was

298 predicted by modelling to compete at least in part for the sugar acceptor site on the enzyme

299 (Byrne et al. 2018b). This was consistent with the documented ability of suramin to compete

300 with, for example, the binding of FGF2 to heparan sulfate (Fernig et al. 1992). The observation

301 that suramin was also an inhibitor of tyrosylprotein sulfotransferase 1 (Byrne et al. 2018a),

302 however, suggested that suramin might be a fairly generic sulfotransferase inhibitor that

303 competed with the universal sulfate donor PAPS. We therefore tested whether suramin would

304 compete for GST-HS3ST3A1 binding to heparin. Suramin was premixed with 50 nM

305 HS3ST3A1 to provide the indicated final concentrations (Fig. 6). The data demonstrate a dose-

306 dependent inhibition of heparin binding by suramin with an IC_{50} of around 5 µM (Fig. 5A). This

307 provides experimental support for the modelling studies presented previously (Byrne et al.

308 2018b). Thus, the heparin derivatised surface also provides the means to identify compounds that

309 compete for the polysaccharide acceptor substrate that are likely to be inhibitors of the HSSTs.

310

Conclusions

312 The surface assembled here provides a versatile means by which to capture biotinylated ligands

313 and is characterised by a low level of non-specific binding. At each stage of assembly, these

314 surfaces may be stored and, in the case of the final heparin functionalised surface, re-used and

315 are resistant to a range of regeneration methods. The thiolated OEG/thiolated biotin OEG

316 surfaces can be stored at 4°C in ethanol for at least three months, while streptavidin and the

317 biotin heparin functionalised surfaces can be stored at 4 °C in PBS for at least 10 days, and the

318   latter re-used over a week. Moreover, functionalised surfaces can be plasma cleaned and re-used

319   2-3 times. Consequently, these surfaces are entirely compatible with the low cost and portability

320   of the instrument and provide an alternative to the peptide surface employed previously e.g.,

321   (Bolduc et al. 2009; Bolduc et al. 2011; Bolduc et al. 2010). The stability of the heparin

322   derivatised surface makes this an interesting route to the development of generic capture surfaces

323   for 'sandwich' type assays, since many proteins associated with pathological changes (Nunes et

324   al. 2019; Salamat-Miller et al. 2007) including viral ones bind heparin, a close structural

325   analogue of the naturally occurring cell surface receptor for many viruses, including SARS-CoV-

326   2 (Kim et al. 2020; Liu et al. 2021; Mycroft-West et al. 2020).

327

Acknowledgements
328

329   We thank Richard Nichols, Department of   Chemistry, Univeristy of Liverpool for training

332   and access to a plasma cleaner during   lockdown.

333

References
334

335   Bolduc OR, Clouthier CM, Pelletier JN, and Masson JF. 2009. Peptide self-assembled monolayers
336   for label-free and unamplified surface plasmon resonance biosensing in crude cell
337   lysate. *Anal Chem* 81:6779-6788. 10.1021/ac900956y

338   Bolduc OR, Lambert-Lanteigne P, Colin DY, Zhao SS, Proulx C, Boeglin D, Lubell WD, Pelletier JN,
339   Fethiere J, Ong H, and Masson JF. 2011. Modified peptide monolayer binding His-tagged
340   biomolecules for small ligand screening with SPR biosensors. *Analyst* 136:3142-3148.
341   10.1039/c1an15235a

342   Bolduc OR, Pelletier JN, and Masson JF. 2010. SPR Biosensing in crude serum using ultralow
343   fouling binary patterned peptide SAM. *Anal Chem* 82:3699-3706. 10.1021/ac100035s

344   Brigham-Burke M, Edwards JR, and O'Shannessy DJ. 1992. Detection of receptor-ligand
345   interactions using surface plasmon resonance: model studies employing the HIV-1
346   gp120/CD4 interaction. *Anal Biochem* 205:125-131. 10.1016/0003-2697(92)90588-x

347   Byrne DP, Li Y, Ngamlert P, Ramakrishnan K, Eyers CE, Wells C, Drewry DH, Zuercher WJ, Berry
348   NG, Fernig DG, and Eyers PA. 2018a. New tools for evaluating protein tyrosine sulfation:
349   tyrosylprotein sulfotransferases (TPSTs) are novel targets for RAF protein kinase
350   inhibitors. *Biochemical Journal* 475:2435-2455. 10.1042/Bcj20180266

351   Byrne DP, Li Y, Ramakrishnan K, Barsukov IL, Yates EA, Eyers CE, Papy-Garcia D, Chantepie S,
352   Pagadala V, Liu J, Wells C, Drewry DH, Zuercher WJ, Berry NG, Fernig DG, and Eyers PA.
353   2018b. New tools for carbohydrate sulfation analysis: heparan sulfate 2-O-
354   sulfotransferase (HS2ST) is a target for small-molecule protein kinase inhibitors.
355   *Biochem J* 475:2417-2433. 10.1042/BCJ20180265

356   Delehedde M, Lyon M, Gallagher JT, Rudland PS, and Fernig DG. 2002. Fibroblast growth factor-
357   2 binds to small heparin-derived oligosaccharides and stimulates a sustained

358   phosphorylation of p42/44 mitogen-activated protein kinase and proliferation of rat
359   mammary fibroblasts. *Biochem J* 366:235-244. 10.1042/BJ20011718

360 Duchesne L, Octeau V, Bearon RN, Beckett A, Prior IA, Lounis B, and Fernig DG. 2012. Transport
361   of fibroblast growth factor 2 in the pericellular matrix is controlled by the spatial
362   distribution of its binding sites in heparan sulfate. *PLoS Biol* 10:e1001361.
363   10.1371/journal.pbio.1001361

364 Edwards PR, Gill A, Pollard-Knight DV, Hoare M, Buckle PE, Lowe PA, and Leatherbarrow RJ.
365   1995. Kinetics of protein-protein interactions at the surface of an optical biosensor. *Anal*
366   *Biochem* 231:210-217. 10.1006/abio.1995.1522

367 Ferhan AR, Yoon BK, Park S, Sut TN, Chin H, Park JH, Jackman JA, and Cho NJ. 2019. Solvent-
368   assisted preparation of supported lipid bilayers. *Nat Protoc* 14:2091-2118.
369   10.1038/s41596-019-0174-2

370 Fernig DG, Rudland PS, and Smith JA. 1992. Rat mammary myoepithelial-like cells in culture
371   possess kinetically distinct low-affinity receptors for fibroblast growth factor that
372   modulate growth stimulatory responses. *Growth Factors* 7:27-39.
373   10.3109/08977199209023935

374 Kim SY, Jin W, Sood A, Montgomery DW, Grant OC, Fuster MM, Fu L, Dordick JS, Woods RJ,
375   Zhang F, and Linhardt RJ. 2020. Characterization of heparin and severe acute respiratory
376   syndrome-related coronavirus 2 (SARS-CoV-2) spike glycoprotein binding interactions.
377   *Antiviral Res* 181:104873. 10.1016/j.antiviral.2020.104873

378 Li Y, Sun CY, Yates EA, Jiang C, Wilkinson MC, and Fernig DG. 2016. Heparin binding preference
379   and structures in the fibroblast growth factor family parallel their evolutionary
380   diversification. *Open Biology* 6. ARTN 150275
381 10.1098/rsob.150275

382 Liu L, Chopra P, Li X, Bouwman KM, Tompkins SM, Wolfert MA, de Vries RP, and Boons GJ. 2021.
383   Heparan Sulfate Proteoglycans as Attachment Factor for SARS-CoV-2. *ACS Cent Sci*
384   7:1009-1018. 10.1021/acscentsci.1c00010

385 Marques JT, de Almeida RFM, and Viana AS. 2014. Lipid bilayers supported on bare and
386   modified gold - Formation, characterization and relevance of lipid rafts. *Electrochimica*
387   *Acta* 126:139-150. 10.1016/j.electacta.2013.07.117

388 Mauriz E, Calle A, Montoya A, and Lechuga LM. 2006. Determination of environmental organic
389   pollutants with a portable optical immunosensor. *Talanta* 69:359-364.
390   10.1016/j.talanta.2005.09.049

391 Migliorini E, Thakar D, Sadir R, Pleiner T, Baleux F, Lortat-Jacob H, Coche-Guerente L, and
392   Richter RP. 2014. Well-defined biomimetic surfaces to characterize glycosaminoglycan-
393   mediated interactions on the molecular, supramolecular and cellular levels. *Biomaterials*
394   35:8903-8915. 10.1016/j.biomaterials.2014.07.017

395 Moon AF, Edavettal SC, Krahn JM, Munoz EM, Negishi M, Linhardt RJ, Liu J, and Pedersen LC.
396   2004. Structural analysis of the sulfotransferase (3-o-sulfotransferase isoform 3)
397   involved in the biosynthesis of an entry receptor for herpes simplex virus 1. *J Biol Chem*
398   279:45185-45193. 10.1074/jbc.M405013200

399 Mycroft-West CJ, Su D, Pagani I, Rudd TR, Elli S, Gandhi NS, Guimond SE, Miller GJ, Meneghetti
400   MCZ, Nader HB, Li Y, Nunes QM, Procter P, Mancini N, Clementi M, Bisio A, Forsyth NR,
401   Ferro V, Turnbull JE, Guerrini M, Fernig DG, Vicenzi E, Yates EA, Lima MA, and Skidmore

402   MA. 2020. Heparin Inhibits Cellular Invasion by SARS-CoV-2: Structural Dependence of
403   the Interaction of the Spike S1 Receptor-Binding Domain with Heparin. *Thromb Haemost*
404   120:1700-1715. 10.1055/s-0040-1721319

405 Nunes QM, Su D, Brownridge PJ, Simpson DM, Sun C, Li Y, Bui TP, Zhang X, Huang W, Rigden DJ,
406   Beynon RJ, Sutton R, and Fernig DG. 2019. The heparin-binding proteome in normal
407   pancreas and murine experimental acute pancreatitis. *PLoS One* 14:e0217633.
408   10.1371/journal.pone.0217633

409 Rahmoune H, Chen HL, Gallagher JT, Rudland PS, and Fernig DG. 1998. Interaction of heparan
410   sulfate from mammary cells with acidic fibroblast growth factor (FGF) and basic FGF.
411   Regulation of the activity of basic FGF by high and low affinity binding sites in heparan
412   sulfate. *J Biol Chem* 273:7303-7310. 10.1074/jbc.273.13.7303

413 Sadir R, Forest E, and Lortat-Jacob H. 1998. The heparan sulfate binding sequence of interferon-
414   gamma increased the on rate of the interferon-gamma-interferon-gamma receptor
415   complex formation. *J Biol Chem* 273:10919-10925. 10.1074/jbc.273.18.10919

416 Salamat-Miller N, Fang J, Seidel CW, Assenov Y, Albrecht M, and Middaugh CR. 2007. A
417   network-based analysis of polyanion-binding proteins utilizing human protein arrays. *J
418   Biol Chem* 282:10153-10163. 10.1074/jbc.M610957200

419 Schuck P, and Zhao H. 2010. The role of mass transport limitation and surface heterogeneity in
420   the biophysical characterization of macromolecular binding processes by SPR
421   biosensing. *Methods Mol Biol* 627:15-54. 10.1007/978-1-60761-670-2_2

422 Su D, and Fernig DG. 2021. Preparation of oleylethylene glycol-sreptavidin surfaces for SPR.
423   *Available at dx.doi.org/10.17504/protocols.io.byv9pw96*.

424 Thakar D, Migliorini E, Coche-Guerente L, Sadir R, Lortat-Jacob H, Boturyn D, Renaudet O, Labbe
425   P, and Richter RP. 2014. A quartz crystal microbalance method to study the terminal
426   functionalization of glycosaminoglycans. *Chem Commun (Camb)* 50:15148-15151.
427   10.1039/c4cc06905f

428 Watts HJ, Lowe CR, and Pollard-Knight DV. 1994. Optical biosensor for monitoring microbial
429   cells. *Anal Chem* 66:2465-2470. 10.1021/ac00087a010

430 Wheeler S, Butler S, Fernig D, Li Y, Hewitt SH, Breen C, and Robertson E. 2021. Anion binding to
431   a cationic europium(III) probe enables the first real-time assay of heparan
432   sulfotransferase activity. *Org Biomol Chem. 2021;DOI: 10.1039/D1OB02071D*.

433 Yates EA, Santini F, Guerrini M, Naggi A, Torri G, and Casu B. 1996. 1H and 13C NMR spectral
434   assignments of the major sequences of twelve systematically modified heparin
435   derivatives. *Carbohydr Res* 294:15-27. 10.1016/s0008-6215(96)90611-4

436 Zhao SS, Bukar N, Toulouse JL, Pelechacz D, Robitaille R, Pelletier JN, and Masson JF. 2015.
437   Miniature multi-channel SPR instrument for methotrexate monitoring in clinical
438   samples. *Biosens Bioelectron* 64:664-670. 10.1016/j.bios.2014.09.082

439

Nomenclature of chemically modified heparin structures

Analogue	Predominant repeat	IdoA-2	GlcN-6	GlcN-2	IdoA-3	GlcN-3
1(heparin)	$I_{2S}A^{6S}_{NS}$	SO_3^-	SO_3^-	SO_3^-	OH	OH
2	$I_{2S}A^{6S}_{NAc}$	SO_3^-	SO_3^-	$COCH_3$	OH	OH
3	$I_{2OH}A^{6S}_{NS}$	OH	SO_3^-	SO_3^-	OH	OH
4	$I_{2S}A^{6OH}_{NS}$	SO_3^-	OH	SO_3^-	OH	OH
5	$I_{2OH}A^{6S}_{NAc}$	OH	SO_3^-	$COCH_3$	OH	OH
6	$I_{2S}A^{6OH}_{NAc}$	SO_3^-	OH	$COCH_3$	OH	OH
7	$I_{2OH}A^{6OH}_{NS}$	OH	OH	SO_3^-	OH	OH
8	$I_{2OH}A^{6OH}_{NAc}$	OH	OH	$COCH_3$	OH	OH
9	$I_{2S,3S}A^{6S}_{3S,NS}$	SO_3^-	SO_3^-	SO_3^-	SO_3^-	SO_3^-

I denotes L-iduronate (IdoA), and A stands for the amino sugar, D-glucosamine (GlcN). Numbers refer to the ring position of the carbon atoms, OH denotes free hydroxyl, S, sulfate ester and NAc or NS represent N-acetylation of N-sulfation of the amino group of glucosamine, respectively.

Figure 1

Schematic of the assembly of the OEG self-assembled monolayer and subsequent capture of streptavidin and biotinylated ligand

Left, illustration of the effect of reducing the mole percentage biotin OEG in the self-assembled monolayer on the density of streptavidin compared to (right) the densely packed streptavidin layer formed on a 1 % (mole/mole) biotin OEG self-assembled monolayer. The latter results in the formation of a 'brush' of an end-labelled polymer, illustrated with reducing end biotinylated heparin.
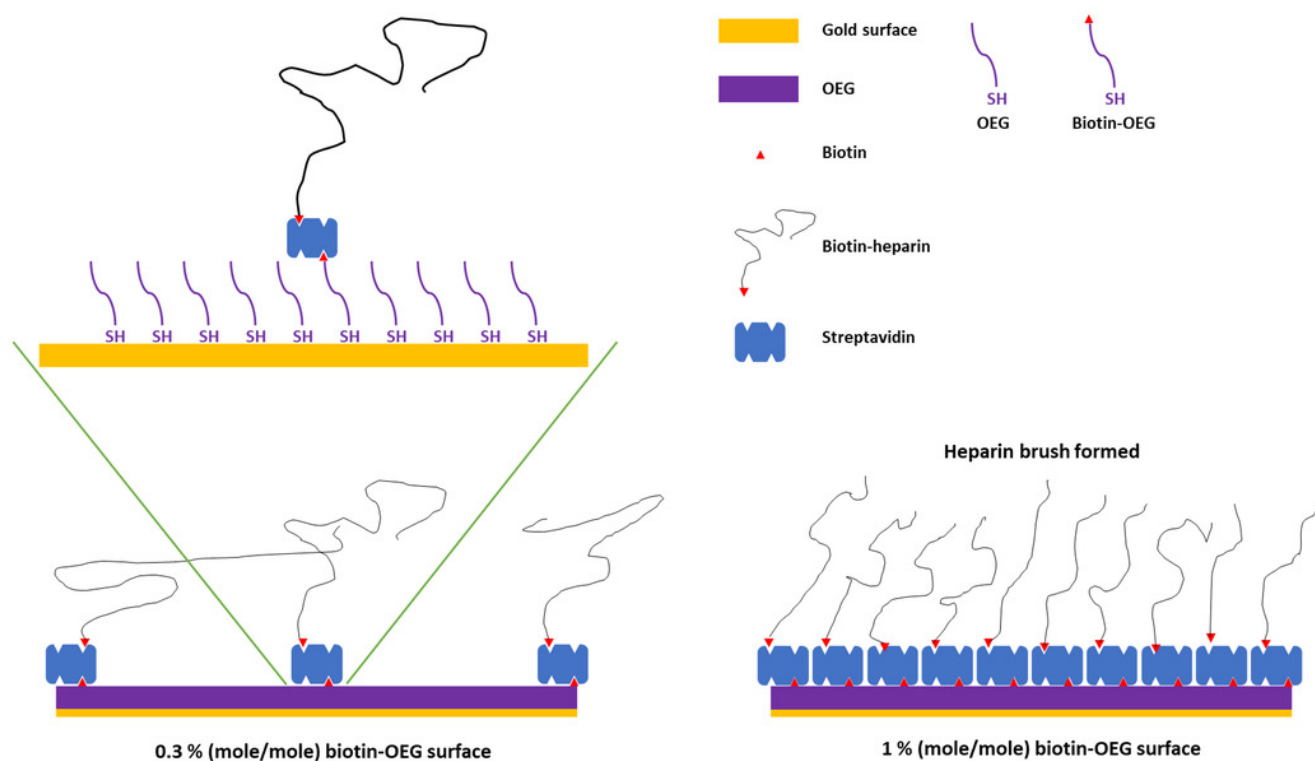
Figure 2

Capture of streptavidin on biotin OEG/OEG self-assembled monolayers and functionalisation with reducing end biotinylated heparin

Following *ex-situ* assembly of the biotin OEG/OEG monolayer, the chip was inserted into the P4SPR instrument and a flow rate of 500 µL/min PBS was maintained. (A) One mL of 20 µg/mL streptavidin in PBS was injected over a 1 % (mole/mole) biotin OEG/OEG SAM in channels A-C and D, after which unbound streptavidin was removed by a 1 mL wash with 2 M NaCl in 10 mM (buffer), pH 7.2, and, after returning the surface to PBS with 1 mL 20 mM HCl. A repeat injection of 1 mL 20 µg/mL streptavidin in PBS over channels A-C and D (800 min, red arrows, inset) did not result in the capture of any further streptavidin on the surface. (B) Reducing end biotinylated heparin (90 µg/mL) was injected over the streptavidin derivatised a 1% (mole/mole) biotin OEG SAM in channels A-C from panel (A). After washing the surfaces with 2 M NaCl and 20 mm HCl to remove any loosely bound biotin heparin, a second injection of reducing end biotin (90 µg/mL) was performed over channels A-C, (2260 min, red arrows, inset. (C) Effect of altering the mole percentage of biotin OEG in the SAM on the amount of streptavidin captured. Three surfaces with SAMs assembled using the indicated mole percentage biotin OEG were prepared. (1 mL, 20 µg/mL) was injected over the surfaces. The traces from each experiment are superimposed to enable comparison. Data for the three measurement channels A-C are the mean of the response in these channels.
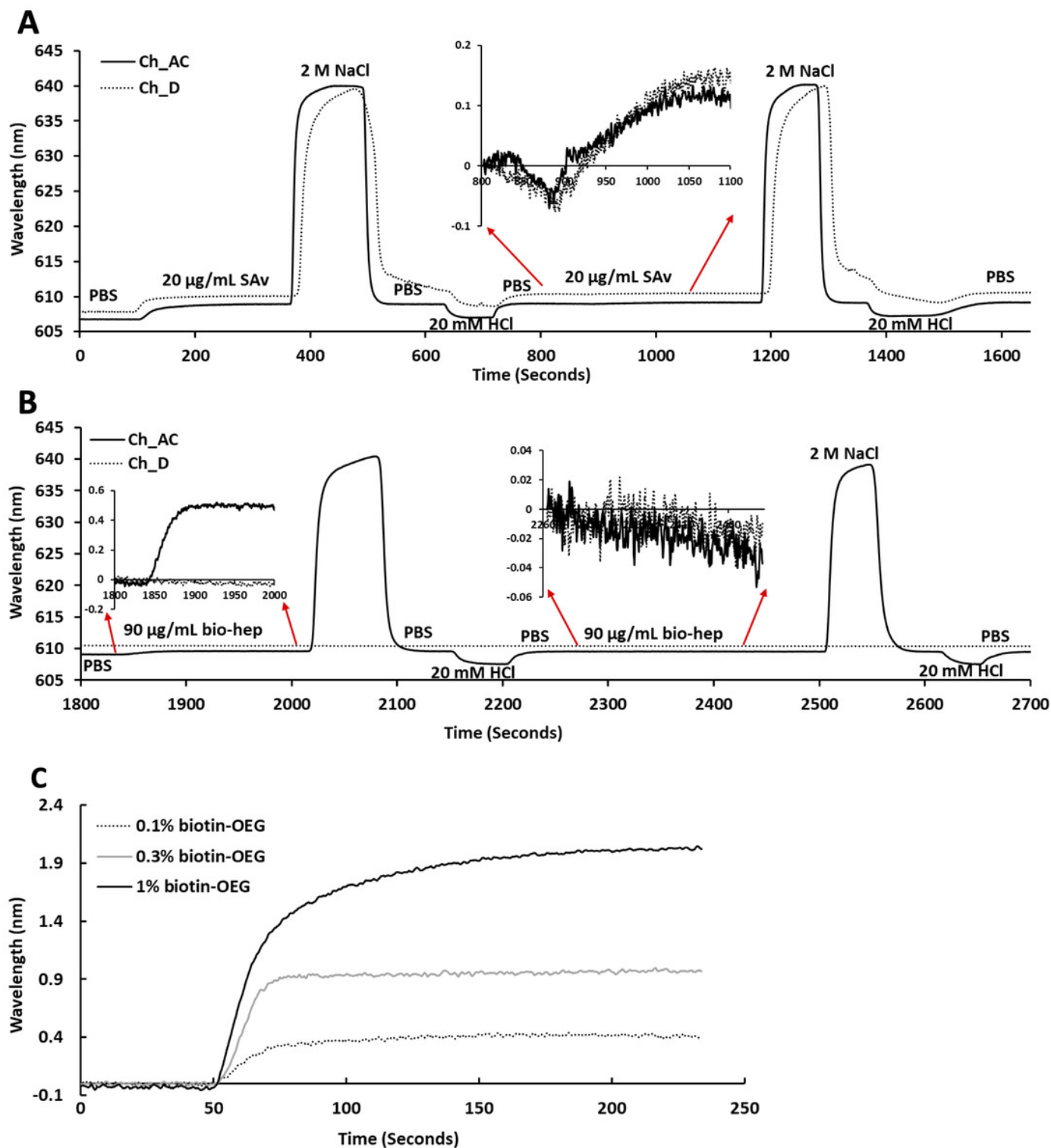
Figure 3

Binding of FGF2 and GST-HS3ST3A1 to a heparin derivatised surface

Streptavidin was captured on a 1% (mole/mole) biotin OEG SAM and reducing end biotinylated heparin was in turn captured on channels A-C, leaving channel D as the control for non-specific binding, as in Fig. 2B. The flow rate of PBST over the surface was maintained at 500 µL/min. (A) 1 mL 100 nM FGF2 was injected over channels A-C (biotinylated heparin) and channel D (streptavidin), followed by regeneration of the surface by sequential washes with 1 mL 2 M NaCl and 20 mM HCl. (B) 1 mL 50 nM GST-HS3ST3A1, followed by regeneration with 2 M NaCl and 20 mM HCl. Inset: expanded view of GST-HS3ST1A1 binding. (C) 1 mL 50 nM GST-HS3ST3A1, followed by regeneration with 1mL injection of 0.25 % (w/v) SDS and then 20 mM HCl.
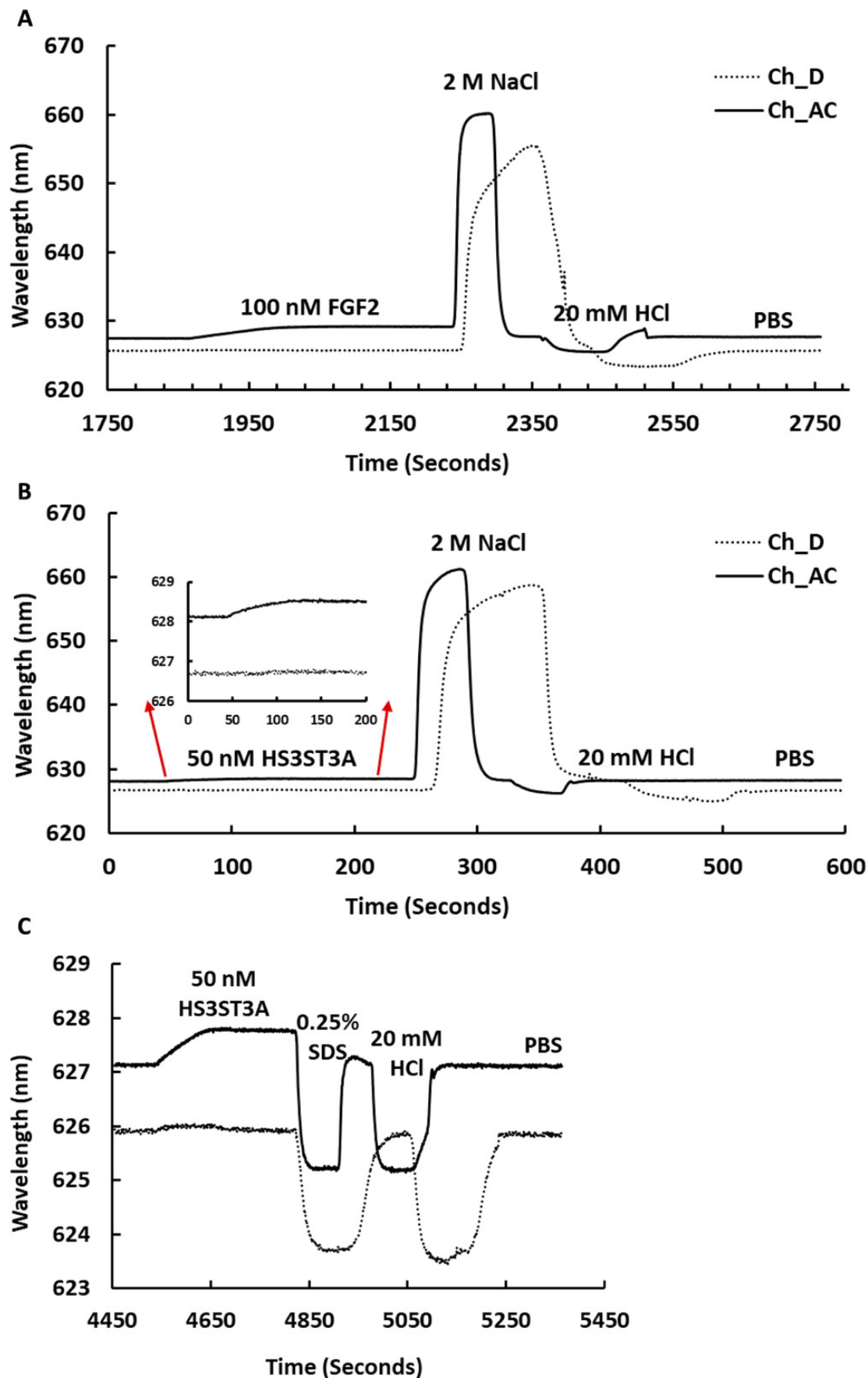
Figure 4

Dissociation induced by soluble heparin

Channels A-C on a chip with streptavidin captured on a 1% mole/mole biotin OEG SAM were functionalised with biotinylated heparin. 1 mL (A) 100 mM FGF2 and (B) 100 mM GST-HS3ST3A1 were injected at 500 µL/min. After the surface was returned to running buffer 1 mL heparin in PBS was injected over the surface.

 Chemistry Journals
Analytical, Inorganic, Organic, Physical, Materials Science
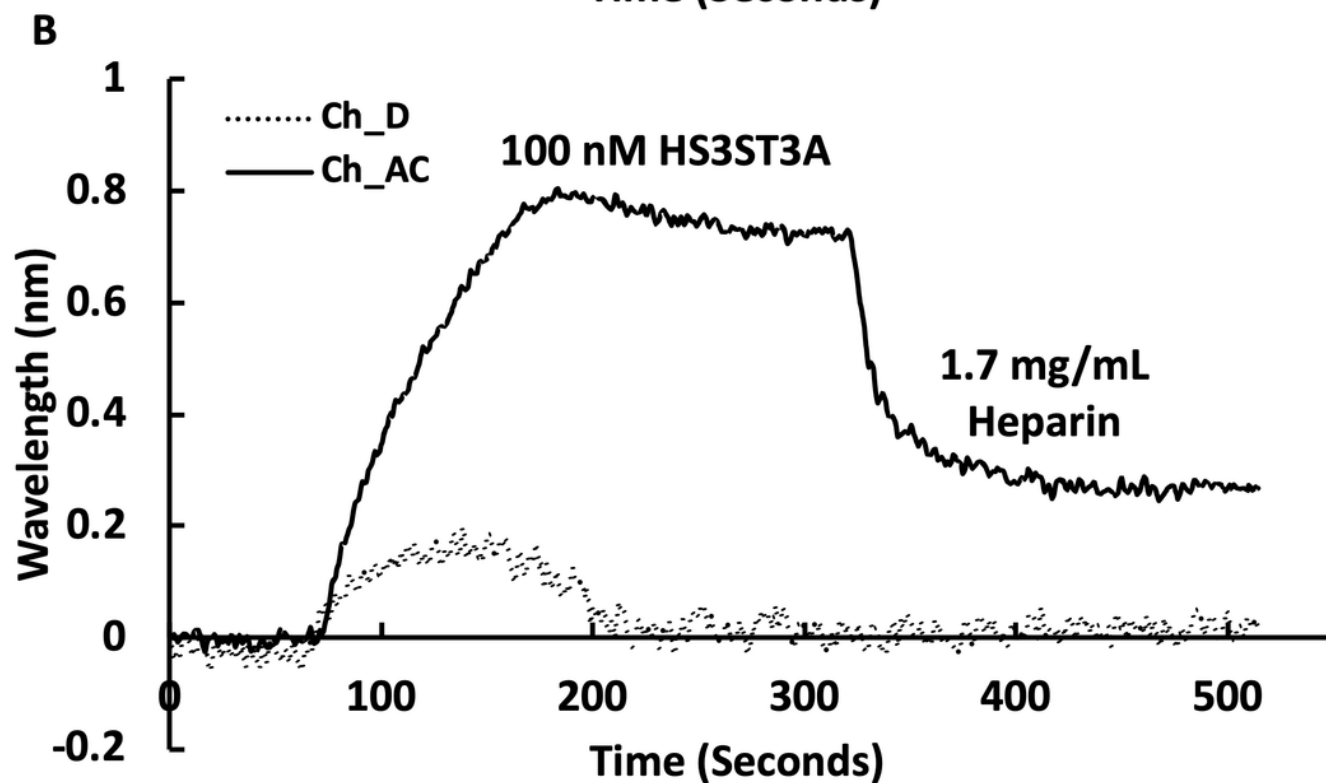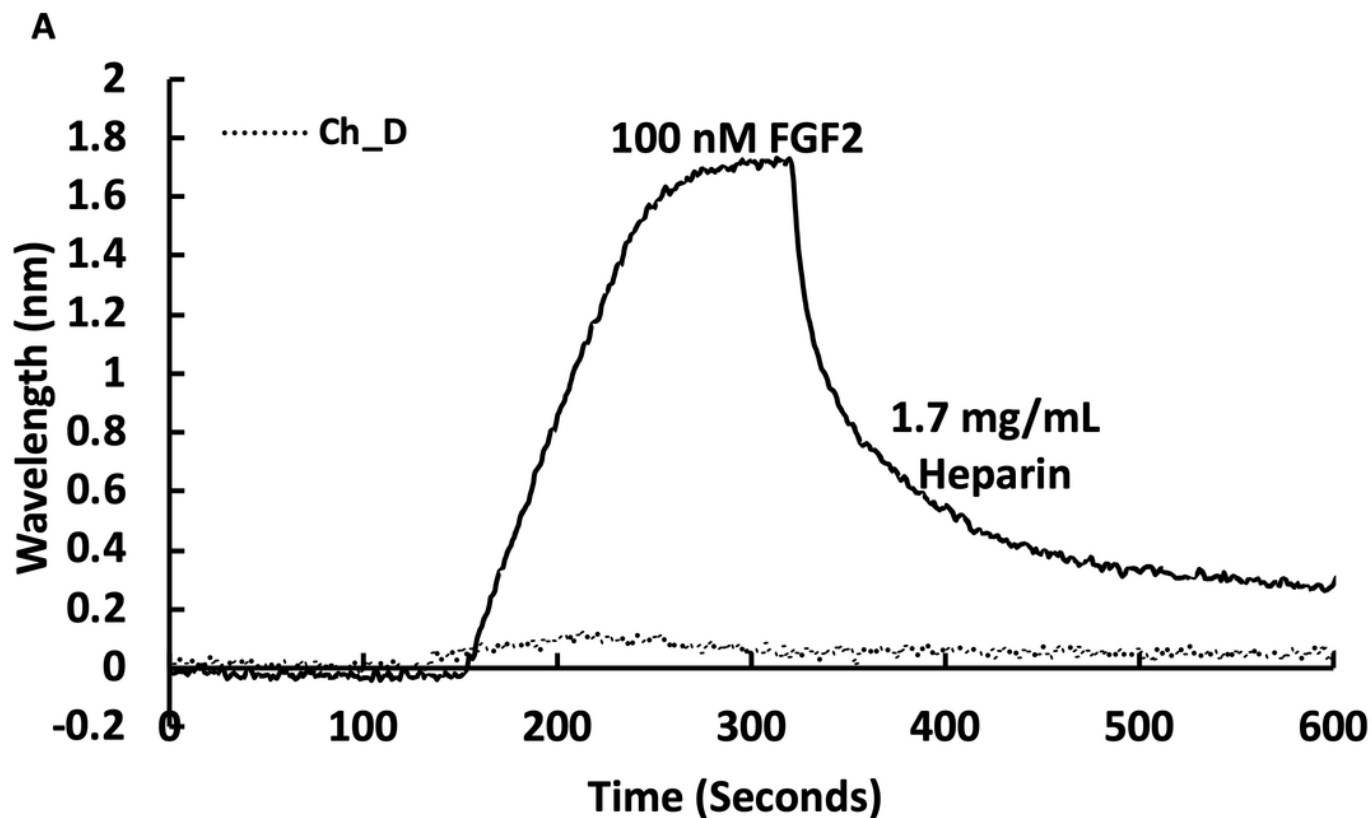
Figure 5

Competition by heparin derivatives for HS3STA1 binding to immobilised heparin

Channels A-C on a chip with streptavidin captured on a 1% mole/mole biotin OEG SAM were functionalised with biotinylated heparin. GST-HS3ST3A1 (50 nM, 1 mL) mixed with increasing concentrations of (A) heparin, and (B) 1.7 µg/mL heparin and heparin derivatives (Table 1). Between each injection the surface was regenerated by a 1 mL injection of 2 M NaCl followed by 1 mL 20 mM HCl. The response was the difference in nm of signal between the initial baseline in PBST and the baseline achieved after the surface returned to PBST following the injection of analyte; the percentage binding was calculated with respect to the response in the absence of added competitor. The data in this figure and in Figure 6 were acquired on the same surface. All values were measured by a single injection over the three measurement channels, so as triplicate technical repeats. However, the control values for 50 nM GST-HS3ST3A1 were determined independently eight times, twice at the start, then every fourth injection, to ensure the surface was responding consistently throughout. The control value is, therefore, the mean of eight independent triplicate repeats and is the same for Panels (A) and (B) and for Figure 6. Error bars are the means ±SD.
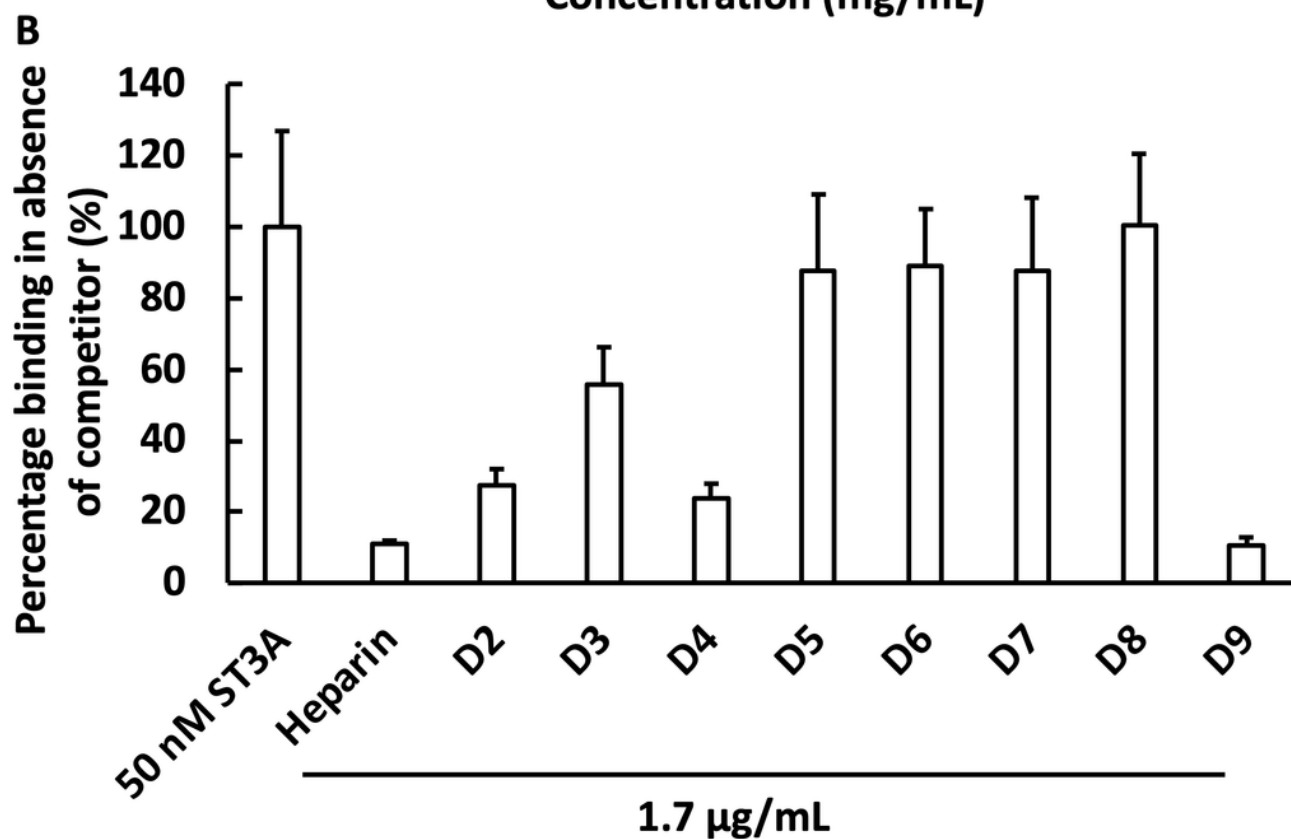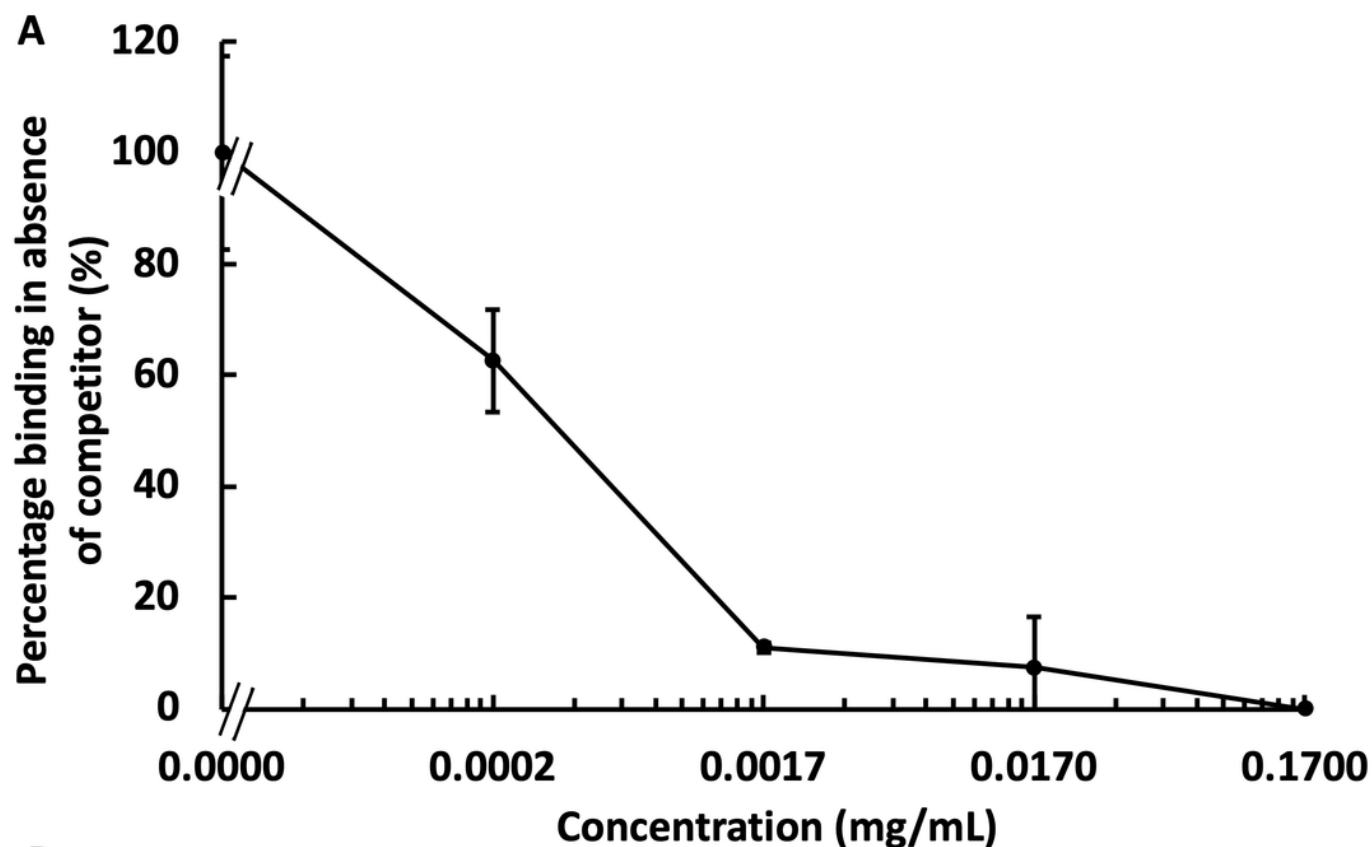
Figure 6

Competition by suramin for GST-HS3ST3A1 binding to immobilised heparin

One mL 50 nM GST-HS3ST3A1 in the presence of increasing concentrations of suramin was injected over a heparin functionalised surface. The response measured was the difference in nm of signal between the initial baseline in PBST and the baseline achieved after the surface returned to PBST following the injection of analyte. Results are the mean ±SD of three technical repeats and are expressed as a percentage of the response measured in the absence of suramin, which was determined in eight independent triplicate repeats, and is the same as that in Figure 5.